Available online at www.sciencedirect.com
SCIENCE DIRECT®
Journal of Chromatography A, 982 (2002) 69–84
JOURNAL OF CHROMATOGRAPHY A
www.elsevier.com/locate/chroma

Co-eluent effect in partition chromatography. Rhamnose–xylose separation with strong and weak cation-exchangers in aqueous ethanol

Jari Tiihonen[a,*], Tuomo Sainio[a], Ari Kärki[b], Erkki Paatero[a]

[a]*Lappeenranta University of Technology, Laboratory of Industrial Chemistry, P.O. Box 20, FIN-53851 Lappeenranta, Finland*
[b]*Danisco Sugar and Sweeteners, 02460 Kantvik, Finland*

Received 2 July 2002; received in revised form 18 September 2002; accepted 19 September 2002

Abstract

The effect of ethanol in aqueous eluent on the chromatographic separation was studied at 298 K. Two sugars, L-rhamnose and D-xylose, were separated by using strong and weak cation-exchangers as a stationary phase. The ionic form of the resins was Na^+ or Ca^{2+}. The separations were carried out with sugar feed concentrations up to 35 wt% and with both low (about 1%) and high (about 10%) feed volume to bed volume ratios. The separation of the sugars was improved by adding ethanol into the eluent. The separation was also significantly enhanced when the weak cation-exchangers with the greatest affinity for water were used instead of strong cation-exchangers as a separation medium for the sugars having different hydrophilicities. The experimental data were successfully explained with a rate-based column model, which accounted for the volume changes of the stationary phase. A thermodynamic sorption model was utilized in column calculations.

Keywords: Mobile phase composition; Cation-exchangers; Rhamnose; Xylose; Ethanol

1. Introduction

Production-scale chromatographic separations in sugar industry are conventionally carried out with strong sulfonated cation-exchangers (SCE) [1]. A typical example is the glucose–fructose fractionation. Weak acrylic cation-exchangers (WCE) are not known to be used in sugar industry as a chromatographic medium but they are applied in ash removal and decolorizing of sucrose containing sugar syrups or in deionization processes either alone or together with anion-exchangers in mixed beds [2,3]. Recently, an industrial application for sugar separation with weak cation-exchangers has been proposed [4]. Moreover, the conventional unit operations have been implemented using water as eluent, and references to separation of carbohydrates as well as other compounds in concentrated ethanol eluents are limited to dilute solutions in analytical scale [5,6].

At concentrated ethanol solutions, the carbohydrate solubility is drastically reduced and at the same time the salt forms of ion-exchangers are strongly deswelled which brings about slower diffusion rates in the resin phase [7–9]. Furthermore, the retention times increase markedly at concentrated ethanol solutions due to increased sorption of carbohydrates

*Corresponding author. Tel.: +358-5-621-2259; fax: +358-5-621-2199.
E-mail address: jari.tiihonen@lut.fi (J. Tiihonen).

0021-9673/02/$ – see front matter
PII: S0021-9673(02)01522-4

into the ion-exchangers [6]. These factors make the larger scale separation at concentrated ethanol eluents less appealing. Thus, relatively low ethanol concentrations were studied to retain reasonably high carbohydrate solubility and still make use of the enhanced separation due to the aqueous ethanol eluent.

In this paper, the suitability of aqueous ethanol and the effect of the resin matrix on sugar separations from concentrated sugar solutions are studied. The experimental chromatographic data of rhamnose–xylose separation has been simulated with a column model. Rate-based models have been commonly used in column calculations [10] and a rate-based model will also be used here. The essential part of the column calculation is the sorption isotherm model. In practice, the isotherms used in column calculations vary from one component linear isotherm equation to multicomponent non-linear isotherm models such as multicomponent Langmuir or Langmuir–Freundlich type equations [10]. These approaches are either empirical or are based on the analogy with surface adsorption, and are not related to the physical properties of the swollen polymer resins. More realistic thermodynamic sorption models are frequently used in equilibrium studies of polymer gels. However, they have been rarely included in column calculations; Lisec et al. and Mazzotti et al. used such an approach for modelling reactive chromatography [11,12]. The thermodynamic sorption model reported in Tiihonen et al. [7] has been utilized here in calculations of the chromatographic data.

In the present paper, new data on sugar separation in aqueous ethanol eluents are reported. In addition to the conventional separation with differently cross-linked SCE (Na^+, Ca^{2+}) also the separation with different cross-linkage WCE (Na^+) is considered.

2. Experimental

2.1. Materials

The stationary phases used were strong poly-(styrene-*co*-divinylbenzene) (PS–DVB) cation-exchangers (SCE) CS08G, CS11G and CS16G and weak acrylic cation-exchangers (WCE) CA06G, CA08G, and CA12G. The resins are manufactured by Finex Oy (Finland). The stationary phases were mainly used in the Na^+ form. The strong cation-exchangers were also studied in the Ca^{2+} form. The functional group of the SCE resins is sulfonic acid and that of the WCE resins carboxylic acid. The characteristics of the resins can be found from Table 1. The nominal degree of cross-linking for the SCE and WCE resins is given as a weight percentage of divinylbenzene (DVB) in the monomer mixture. The ion-exchange procedures were carried out by using reagent-grade electrolytes.

The sugars studied were L-rhamnose monohydrate (Kaden Biochemicals) and D-xylose (Xyrofin, Fin-

Table 1
Properties of the stationary phases

Resin name	Resin type	Ionic forms studied	Cross-linkage, wt% of DVB	d_{av}[a] (mm)	Capacity in Na^+ form (mequiv/g)	Water retention (wt%)	q[c] = V_{water}/V_{dry}, (m^3/m^3)	G[d] (MPa)
CS08G	SCE ×4	Na^+, Ca^{2+}	4	0.35	4.5	65[b]	3.6[b]	3.8[b]
CS11G	SCE ×5.5	Na^+	5.5	0.39	4.6	56	2.7	9.6
CS16G	SCE ×8	Na^+, Ca^{2+}	8	0.35	4.7	47[b]	2.1[b]	21[b]
CA08G	WCE ×4	Na^+	4	0.39	9.6	76	6.2	4.1
CA12G	WCE ×6	Na^+	6	0.39	9.3	70	4.8	7.9

WCE, weak cation-exchanger; SCE, strong cation-exchanger.
[a] Average bead diameter in Na^+ form in water.
[b] Na^+ form.
[c] Swelling ratio in water.
[d] Shear modulus of the water-swollen polymer.

land). The non-sorbed component was Blue Dextran 2000 ($2 \cdot 10^6$ g/mol, Amersham Pharmacia Biotech AB). Ethanol (about 94 or 99.5 wt%, Primalco, Finland) was diluted with ion-exchanged water to the level used in the eluent or in the sorption equilibrium studies. All solutions were prepared in deionized water ($\kappa < 0.5$ μS cm^{-1}).

2.2. Methods

The desired ionic form of the resins was obtained and the capacity was determined with the methods presented in Tiihonen et al. [13]. The water–ethanol, the water–sugar and the water–ethanol–sugar sorption equilibrium studies were made at 298 K. The details of the measurement procedures can be found in Tiihonen et al. [13,14].

The chromatographic measurements were made with a Pharmacia Biotech FPLC chromatographic system equipped with a thermostated glass column and an RI (RI-98 Scope) detector. The fractions were collected with Pharmacia LKB-FRAC-100 fraction collector. In some cases, only single component experiments were made, and only the RI data was recorded. The diameter of the column was 1.6 cm and the length of the resin bed was 16.9–30.0 cm. The porosity of the bed was determined with Blue Dextran and it was between 0.3 and 0.4. The chromatographic runs were made at 298 K. The eluent composition used was 0, 10 or 30 wt% aqueous ethanol solution. The flow-rate was 0.25 or 1.00 cm^3/min and the column was run in pulse mode. The injection volume of the sample was either 0.5 or 5.5 cm^3 and the concentration of each sugar in the sample varied from 5.3 to 7.0 wt% or from 16 to 19 wt%. Details of the chromatographic runs are given in Table 2. For each resin, the chromatographic runs at different eluent compositions and sample amounts were made with the same bed capacity. The change in bed height is mainly due to the swelling or the deswelling of the resin beads at different eluent compositions. It should be noted, that the dramatic shortening of the WCE Na^+ ×4 resin bed from 30.0 to 16.9 cm, when changing the eluent from water to 29 wt% ethanol, is caused by the strong shrinking of the WCE Na^+ resins in the aqueous ethanol solutions [7].

The ethanol and sugar contents in the fractions collected from the chromatographic runs as well as in the solutions from the water–ethanol–sugar equilibrium measurements were analyzed by means of a HP 1100 series HPLC system equipped with

Table 2
Conditions in the chromatographic runs shown in Figs. 2–5

Resin	Bed height (cm)	Ethanol in eluent (wt%)	Bed porosity	Sample concentration (wt%)		Sample volume (cm^3)	B[a]	Flow-rate (cm^3/min)	Figure
				Rhamnose	Xylose				
SCE Na^+ ×8	26.0	0.0	0.35	5.4	6.1	0.5	0.50	0.25	5A
SCE Na^+ ×5.5	30.0	0.0	0.39	16	18	5.5	0.32	1.0	3A
SCE Na^+ ×5.5	28.7	9.5	0.37	16	19	5.5	0.21	1.0	3B
SCE Na^+ ×5.5	25.5	28	0.30	17	18	5.5	0.20	1.0	2,3C
SCE Na^+ ×5.5	30.0	0.0	0.38	5.4	6.1	0.5	0.55	1.0	4A
SCE Na^+ ×5.5	28.0	9.6	0.33	5.4	6.2	0.5	0.36	1.0	4C
SCE Na^+ ×4	30.3	0.0	0.39	6.3	7.0	0.5	0.70	1.0	5B
SCE Ca^{2+} ×8	26.0	0.0	0.38	5.4	6.1	0.5	0.25	0.25	5D
SCE Ca^{2+} ×4	28.0	0.0	0.39	5.3	6.0	0.5	0.70	0.25	5E
WCE Na^+ ×6	28.0	0.0	0.31	6.3	6.3	0.5	0.45	1.0	5C
WCE Na^+ ×4	30.0	0.0	0.36	16	18	5.5	0.30	1.0	3D
WCE Na^+ ×4	26.4	9.5	0.35	16	18	5.5	0.17	1.0	3E
WCE Na^+ ×4	16.9	29	0.31	16	18	5.5	0.09	1.0	3F
WCE Na^+ ×4	30.0	0.0	0.33	5.5	5.7	0.5	0.50	1.0	4B
WCE Na^+ ×4	25.9	9.5	0.34	5.4	6.1	0.5	0.33	1.0	4D

[a] Coefficient in Eq. (6).

sulfonated PS–DVB (Pb^{2+}) column and an Agilent 1100 series RI detector. The eluent in the HPLC analysis was deionized water.

3. Theory

3.1. Sorption model

The multicomponent sorption isotherms were calculated by a thermodynamic sorption equilibrium model described in detail in Tiihonen et al. [7] and only a brief summary is given here. The chemical potentials of the sorbed species are equal in the liquid phase and in the resin phase at equilibrium. The chemical potential in the liquid phase consists of the mixing effects and in the resin phase of the mixing effects and the elastic effects of the cross-linked polymer matrix (Eq. (1)). System temperature and the pressure of the liquid phase were chosen as the standard state for the chemical potentials in both phases.

$$\ln a_i(l) = \ln a_i(s) + \frac{V_{m,i}}{RT}\pi_{el} \quad (i = 1, n) \tag{1}$$

In Eq. (1) the liquid and the resin phase activities are $a_i(l)$ and $a_i(s)$ of component *i*, respectively. Activity can be calculated from mole fraction and symmetric activity coefficient, i.e. $a_i = x_i\gamma_i$. $V_{m,i}$ is the partial molar volume of component *i* and π_{el} is the elastic pressure. For simplicity, pure component molar volumes are used for all components. *R* and *T* have their usual meanings.

The activity coefficients were calculated by using the non-random factor equation (NRF) [7]. The random mixing was given by the athermal Flory–Huggins equation, and the non-random interactions were expressed by means of the interaction energy parameters ΔE_{ij}. The treatment follows the equation presented originally by Panayiotou and Vera [15] except for the stationary phase. The basic NRF equation was modified by using two different strength binding sites in the ion-exchangers. Both binding sites had their own coordination number, z_i, as shown in Table 3. The sum of the coordination numbers is commonly used 10 [16]. The coordination number z_a or z_b divided by the sum of the coordination numbers represents the surface area fraction of occupied by the corresponding binding site. The elastic pressure appearing in the equilibrium equation was calculated by using an extended Flory elasticity model [17]. The K_{el} in Table 3 is the elastic parameter fitted in the extended Flory elasticity model. K_{el} has a correlation with the experimental shear modulus of the polymer [13,18].

3.2. Column model

A dynamic model for isothermal multicomponent

Table 3
Interaction and elastic parameters of the isotherm model for the water–ethanol–sugar–resin systems

	ΔE_{ij} (J/mol)								
	Water		Ethanol		Rhamnose		Xylose		K_{el} (MPa)
Resin	z_a[a]	z_b[a]	z_a[a]	z_b[a]	z_a[a]	z_b[a]	z_a[a]	z_b[a]	
Water	–	–	230[b]	230[b]	142	142	139	139	–
Ethanol	230[b]	230[b]	–	–	158	158	210	210	–
Rhamnose	142	142	158	158	–	–	0	0	–
SCE Na^+ ×8	421[b]	−1410[b]	119[b]	4.82[b]	515	−2270	467	−2200	11[b]
SCE Na^+ ×5.5	421[b]	−1410[b]	119[b]	4.82[b]	515	−2270	467	−2200	6.1[b]
SCE Na^+ ×4	421[b]	−1410[b]	119[b]	4.82[b]	515	−2270	467	−2200	3.5[b]
SCE Ca^{2+} ×8	606[b]	−1090[b]	176[b]	−172[b]	350	−1180	337	−1080	11[b]
SCE Ca^{2+} ×4	606[b]	−1090[b]	176[b]	−172[b]	350	−1180	337	−1080	3.7
WCE Na^+ ×6	215[b]	−1860[b]	5800[b]	−3920[b]	−400	150	−450	−100	9.0[b]
WCE Na^+ ×4	215[b]	−1860[b]	5800[b]	−3920[b]	−400	150	−450	−100	5.7[b]

[a] Coordination numbers used in the NRF model: z_a is 8 for SCE and 7 for WCE and z_b is 2 for SCE and 3 for WCE.
[b] From Tiihonen et al. [7].

chromatography was derived assuming axially dispersed plug flow conditions. Due to the thermodynamic approach to sorption modeling, none of the components can be regarded as an inert solvent, and the concentrations of all components, including the resin, have to be calculated. Accordingly, the swelling of the resin and the resultant variations in the local porosity cannot be neglected without violating the material balance. The total volume of the bed was held constant, and swelling of the resin was accounted for by letting the bed porosity vary locally with the total sorbed amount. The superficial fluid velocity remains therefore constant, whereas the interstitial fluid velocity varies locally. Mass transfer between the fluid and resin phases was described according to the linear driving force (LDF) model [19] using solid film resistance only. With volume fractions as the concentration variables, the material balance yields the following differential equations for the concentration of component i in liquid and solid-phases [Eqs. (2) and (3)]. Eq. (4) is the continuity condition that relates the local porosity to the total amount sorbed in the resin.

$$\frac{\partial(\epsilon\phi_i^L)}{\partial t} = -u\frac{\partial\phi_i^L}{\partial z} - \frac{\partial\left[(1-\epsilon)\phi_i^S\right]}{\partial t} + D_{ax}\left(\epsilon\frac{\partial^2\phi_i^L}{\partial z^2} + \frac{\partial\phi_i^L}{\partial z}\frac{\partial\epsilon}{\partial z}\right) \quad (2)$$

$$\frac{\partial\left[(1-\epsilon)\phi_i^S\right]}{\partial t} = k_i^{eff}a\left(\hat{\phi}_i^S - \phi_i^S\right),$$

$$k_i^{eff} = \frac{10D_i^S}{d_p^0}\left(\frac{1-\epsilon}{1-\epsilon^0}\right)^{-1/3},$$

$$a = \frac{6}{d_p^0}\left(\frac{1-\epsilon}{1-\epsilon^0}\right)^{-1/3} \quad (3)$$

$$\frac{\partial\epsilon}{\partial t} = -\frac{1}{\phi_P}\sum_{i=1}^{n}\frac{\partial\phi_i^S}{\partial t} \quad (4)$$

In Eqs. (2)–(4), the volume fractions of component i in liquid and resin phases are denoted by ϕ_i^L and ϕ_i^S, and the resin phase volume fraction at sorption equilibrium is denoted by $\hat{\phi}_i^S$. D_{ax} is the axial dispersion coefficient, u the superficial velocity, ϵ the bed porosity, and d_p the particle diameter. k_i^{eff} is the effective mass transfer coefficient, a is the particle area to volume ratio, and D_i^S is the effective solid-phase diffusion coefficient. Both k_i^{eff} and a depend on the extent of swelling, as seen in Eq. (3). The axial coordinate and the time variable are z and t, respectively. It should be noticed that, because of the LDF approximation, ϕ_i^S is an average volume fraction in the resin particle. The constants d_p^0 and ϵ^0 refer to the initial conditions in the column.

3.3. Calculations

3.3.1. Sorption equilibrium calculation procedure

The sorption equilibrium calculations for the water–ethanol–sugar sorption in the cation-exchange resins follow the procedure presented in Ref. [7]. The parameters obtained for water–ethanol–resin systems in Ref. [7] are used, and only parameters needed for sugar sorption are considered here. The water–xylose parameter was calculated from activity coefficient, osmotic coefficient and solubility data (21 data points) [8,20,21]. The corresponding absolute average deviation (AAD) values were 0.78%, 0.46% and 0.03%. The water–rhamnose parameter was calculated from the solubility data [20] with the AAD value 3.33%. The ethanol–xylose parameter was calculated from nine water–ethanol–xylose solubility data points [8] with the AAD value 13.9%. The ethanol–rhamnose parameter was determined from the water–ethanol–rhamnose–resin sorption data measured in our laboratory because of the scarcity of the ethanol–rhamnose data. The xylose–rhamnose parameters were estimated from water–xylose–rhamnose–resin sorption data. A first estimate of the sugar–resin parameters was calculated solely based on the experimental isotherm data. When these parameters were used in the column calculations, significant deviations between experimental and calculated peaks were observed. Therefore, the sugar–resin parameters estimated from the isotherms were slightly modified to give an adequate representation of both the sorption and chromatographic behavior of the system. As seen in Fig. 1, also the modified interaction parameters give a satisfactory fit to the experimental data.

The size and surface parameters as well as the pure component molar volumes for all compounds are given in Table 4. The total volume of the swollen resin was calculated additively from the sorbed amounts and the molar volumes [7]. The interaction

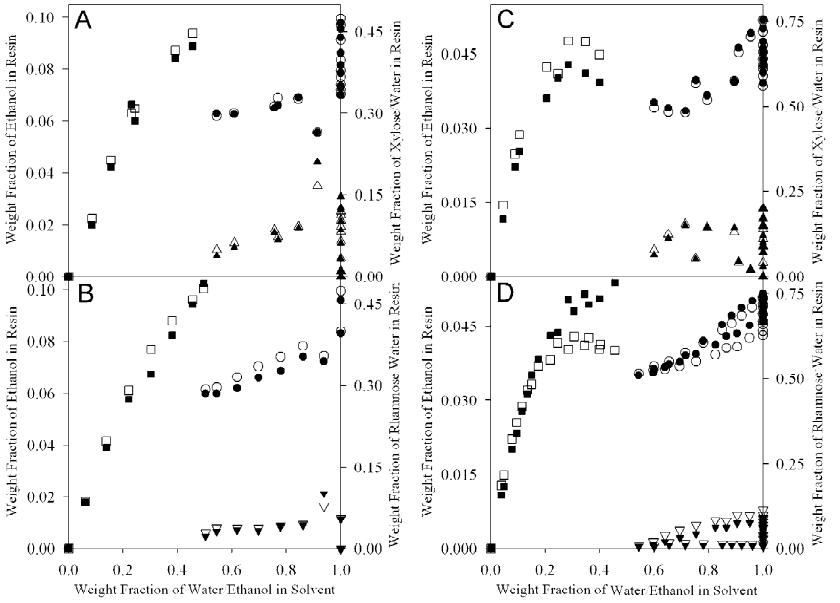

Fig. 1. Example of water–ethanol–sugar sorption on cation-exchangers at 298 K. (A,B) SCE in Na^+ form, ×8. (C,D) WCE in Na^+ form, ×4. Filled symbols represent experimental data points and open symbols have been calculated with the NRF model. Circles are for water, triangles for sugar and squares for ethanol. Water and sugar data has been plotted against water content in solvent and ethanol against ethanol content in solvent.

energy parameters as well as R^2 and AAD values for all systems are given in Tables 3 and 5. The somewhat higher AAD values for rhamnose sorption in the WCE (Table 5) are based on the consistent overprediction in rhamnose sorption (Fig. 1D). The overprediction is due to the compromise of adequate fitting both the sorption data and the chromatographic experiments, as explained above.

Table 4
Size (r_i) and surface (q_i) parameters, pure component molar volumes, $V_{m,i}$, and equivalent volumes, V_{equiv}, for the water ethanol–polymer systems at 298 K

	r_i	q_i	$V_{m,\,i}$ (cm^3/mol)
Water	0.9200[a]	1.400[a]	18
Ethanol	2.576[a]	2.588[a]	58
Rhamnose	7.380[b]	7.028[b]	110
Xylose	6.706[b]	6.492[b]	95
			$V_{equiv,\,i}$ (cm^3/equiv)
SCE Na^+	6000[c]	5000[c]	128[c,d]
SCE Ca^{2+}	6000[c]	5000[c]	123[c,d]
WCE Na^+	3000[c]	2500[c]	58[c,d]

[a] From Peres and Macedo [22].
[b] Estimated from the group contributions in the molecule [23].
[c] From Tiihonen et al. [7].
[d] Same value used for all cross-link densities.

3.3.2. Column calculation procedures

In the present case with four chemical species, Eqs. (2)–(4) form a coupled system of ordinary differential equations (ODE) and hyperbolic–parabolic partial differential equations (PDE). These have to be solved with appropriate boundary conditions and initial values. The Neumann boundary condition, Eq. (5), was used for the spatial derivative of ϕ_i^L at the column inlet because of the dispersive term in Eq. (2). No boundary conditions were used at the column outlet in order to avoid flattening of the traveling fronts. The initial value for the liquid phase composition was equal to the eluent composition everywhere in the column, and that of the resin phase was calculated from the sorption isotherm. The initial value for the bed porosity, ϵ^0, was determined during the chromatography experiments, and that of the particle diameter, d_p^0, was obtained by measuring the degree of swelling of the resin in different eluent compositions.

The PDE system was transferred to a coupled

Table 5
R^2 and AAD values as well as the number of data points, N, for the water–ethanol–sugar–resin systems

Resin	ΔE_{ij} (J/mol)								N
	Water		Ethanol		Rhamnose		Xylose		
	R^2 (%)	AAD (%)	R^2 (%)	AAD (%)	R^2 (%)	AAD (%)	R^2 (%)	AAD (%)	
SCE Na^+ ×8	91.53	3.79	84.62	15.1	88.39	11.8	–	–	11
SCE Na^+ ×8	98.67	1.87	88.62	10.7	–	–	90.24	12.0	18
SCE Na^+ ×5.5[a]	38.40	3.83	–	–	99.33	3.49	–	–	8
SCE Na^+ ×5.5	96.41	2.80	96.85	5.22	–	–	91.75	11.8	16
SCE Na^+ ×4[a]	58.64	3.61	–	–	99.00	4.21	–	–	8
SCE Na^+ ×4	95.55	2.67	99.46	3.30	–	–	89.19	11.8	18
SCE Ca^{2+} ×8	78.94	6.98	99.59	2.49	91.96	8.61	–	–	13
SCE Ca^{2+} ×8	94.83	2.61	99.75	1.53	–	–	92.47	12.7	19
WCE Na^+ ×6[a]	95.14	0.76	–	–	86.34	20.0	–	–	9
WCE Na^+ ×6	96.97	1.82	97.17	3.20	–	–	94.12	7.32	16
WCE Na^+ ×4	92.56	2.77	92.85	8.10	72.65	47.9	–	–	28
WCE Na^+ ×4	98.25	1.76	89.50	8.16	–	–	97.77	8.01	20

[a] Water–rhamnose–polymer data.

system of ODEs according to the finite difference method with a grid spacing of 0.002 m. The resulting initial value problem was solved with an integrator based on the backward differentiation formulas [24]. The spatial derivatives of ϕ_i^L and ϵ were calculated by using five-point Lagrange interpolation polynomials. Due to the hyperbolic nature of the PDE system, biased upwind approximations were used in the interior grid points to avoid oscillation of the numerical solution [25].

$$\frac{\partial \phi_i^L(z=0)}{\partial z} = \frac{u}{D_{ax}}\left[\phi_i^L(z=0) - \phi_i^{feed}(t)\right] \quad (5)$$

Because of the iteration procedures needed to calculate the sorption equilibrium from the NRF model [7], the computing time in chromatographic pulse calculations became excessively long, and a shortcut was needed to decrease the computing time. This was implemented by fitting an explicit equation for each resin to over 400 sorption data points simulated with the activity model. Langmuir–Freundlich (LF) multicomponent isotherm type equation [10] gave excellent accuracy for the conversion (Table 6). It should be noted that, in this case, the LF equation is used only for the isotherm data conversion to the explicit form and its parameter values have no physical meaning. Thus, only R^2 and AAD values of the fits for different resins are shown in Table 6. A typical example of the successful conversion from implicit to explicit isotherm model in column calculation is shown in Fig. 2.

Axial dispersion coefficient was calculated from the correlation of Chung & Wen [26] using average viscosity and density of the eluent, and kept constant despite the swelling of the resin and variations in the

Table 6
R^2 and AAD values of the implicit isotherm model conversion to the explicit form

Resin	R^2 (%)				AAD (%)			
	Water	Ethanol	Rhamnose	Xylose	Water	Ethanol	Rhamnose	Xylose
SCE Na^+ ×8	99.95	99.99	99.99	99.98	0.25	0.33	0.86	0.65
SCE Na^+ ×5.5	99.97	99.99	99.99	99.99	0.22	0.41	0.64	0.61
SCE Na^+ ×4	99.95	99.99	100.0	99.99	0.35	0.34	0.46	0.64
SCE Ca^{2+} ×8	99.92	99.85	99.98	99.99	0.28	0.46	1.01	0.91
SCE Ca^{2+} ×4	99.95	99.94	99.94	99.98	0.36	1.25	1.02	1.01
WCE Na^+ ×6	98.16	99.40	99.99	99.97	1.15	2.30	0.79	1.20
WCE Na^+ ×4	99.63	99.06	99.99	99.94	0.62	2.28	0.80	1.49

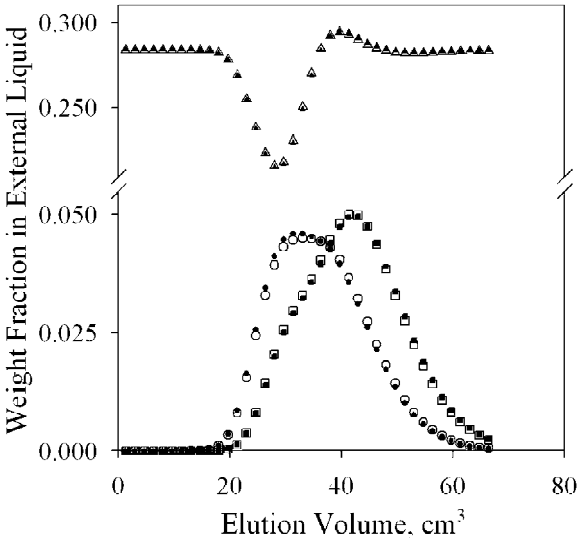

Fig. 2. Chromatograms calculated with the implicit NRF model (filled symbols) and with the NRF model converted to explicit form (open symbols). Resin: SCE Na^+ ×5.5 in 28 wt% aqueous ethanol. Circles are for rhamnose, squares for xylose and triangles for ethanol.

properties of the liquid mixture. The swelling of the resin beads has a two-fold effect on the mass transfer rate: the specific surface area depends on particle size, and the diffusion rates depend on the density of the polymer network. The diffusion coefficient of component i in the solid-phase, D_i^S, was calculated from the volume fraction of the polymer matrix, ϕ_p^S, the diffusion coefficient in water, D_i^{aq}, and a composition dependent coefficient, B (Table 2) according to Eq. (6) [27]. The diffusion coefficients in water are shown in Table 7. The values in Table 7 for water and for ethanol have been got from Refs. [27,28], respectively. The values for sugars in Table 7 have been fitted from a chromatographic run in water eluent with small sample volume and dilute sample. Since possible mass transfer effects in the fluid phase were included in the effective mass transfer coefficient, they are reflected to the effective diffusion coefficient, as seen in Eq. (3). Consequently, the composition dependent constants B in Eq. (6) could be affected by the flow-rate. In the majority of the chromatographic runs, however, a flow-rate of 1.0 cm^3/min has been used (cf. Table 2), and values obtained for the parameter B are comparable. For the SCE resin in Ca^{2+} form, a flow-rate of 0.25 cm^3/min was applied, and the parameter B values at different cross-link densities are comparable.

Table 7
The diffusion coefficients in aqueous solutions (Eq. (6))

Component	D_i^{aq} (10^9 m^2/s)
Water	2.60[a]
Ethanol	1.58[b]
Xylose	0.55[c]
Rhamnose	0.45[c]

[a] Ref. [27].
[b] Ref. [28].
[c] Estimated from the chromatographic run in Fig. 4A with $B=0.55$.

$$D_i^S = BD_i^{aq}\left(\frac{1-\phi_P^S}{1+\phi_P^S}\right)^2 \quad (6)$$

In order to get the needed diffusion parameters [the coefficient B in Eq. (6)] it is necessary to make a few experimental chromatographic runs at selected sample composition or to estimate the coefficient from previous runs with similar stationary phases. In this paper the values of B in Table 2 were estimated from each chromatographic experiment. The conditions of the chromatographic experiments are shown in Table 2.

3.4. Separation efficiency

The efficiency of the rhamnose–xylose separation was described with the separation factor, α, and the peak resolution, R_S [29]. The retention factor, k, in Tables 8 and 9 is the true retention of component i ($V_{R,i}-V_M$) to the retention volume of non-adsorbing component, V_M, ratio. The retention volume, $V_{R,i}$ or V_M, and the peak width, $w_{b,i}$, needed for the parameter determination were calculated with the method of moments [28,30]. Small pulses and dilute sample concentrations were chosen for the moment calculations in order to keep the concentrations at the linear isotherm range and the peaks as ideal as possible.

Table 8
Effect of the resin matrix and eluent composition on the retention factor, k; the width of the peak base, w_b; asymmetry factor, A_S; and diffusional effects, D_i^S, of rhamnose–xylose separation [29]

Resin	Ethanol in eluent (wt%)	k		w_b (cm^3)		A_S		D_i^S (10^{11}m^2/s)		B^a
		Rhamnose	Xylose	Rhamnose	Xylose	Rhamnose	Xylose	Rhamnose	Xylose	
SCE	0	0.37	0.46	6.09	6.29	1.05	1.00	4.2	5.1	0.50
Na^+ ×8	10	0.42	0.55	6.50	6.99	1.06	1.04	3.0	3.7	0.36
	20	0.50	0.69	7.60	8.07	1.23	0.93	2.1	2.5	0.25
	30	0.65	0.96	8.67	9.50	0.99	1.06	1.6	1.9	0.20
SCE	0	0.50	0.61	6.56	6.75	1.09	1.11	6.8	8.3	0.55
Na^+ ×5.5	10	0.56	0.69	6.99	7.46	1.08	1.21	4.5	5.5	0.36
	20	0.65	0.84	7.92	8.44	1.14	1.17	3.1	3.8	0.25
	30	0.81	1.11	8.83	10.1	0.95	1.46	2.5	3.0	0.21
SCE	0	0.64	0.74	6.93	7.17	1.00	0.97	12	14	0.70
Na^+ ×4	10	0.69	0.81	7.29	7.72	1.06	1.08	7.3	8.9	0.43
	20	0.79	0.96	8.15	8.74	1.20	1.00	4.7	5.8	0.28
	30	0.94	1.21	9.06	9.77	1.01	1.18	3.7	4.5	0.23
WCE	0	0.51	0.75	6.36	7.22	0.94	1.03	8.9	11	0.45
Na^+ ×6	10	0.59	0.97	7.29	8.69	0.96	1.05	3.6	4.4	0.20
	20	0.71	1.32	8.76	11.2	0.93	1.09	1.6	1.9	0.10
	30	0.88	1.95	11.4	15.9	0.92	1.11	0.7	0.9	0.06
WCE	0	0.65	0.89	6.87	7.82	1.12	1.01	12	15	0.50
Na^+ ×4	10	0.75	1.14	7.49	9.11	1.12	0.98	7.1	8.7	0.33
	20	0.90	1.54	8.25	11.1	1.08	1.01	3.6	4.5	0.19
	30	1.12	2.27	10.4	15.7	1.08	1.09	1.6	2.0	0.10

Parameters have been calculated from simulated data when small pulses and slow flow-rates were applied.
[a] Coefficient in Eq. (6).

The ideality of the peaks in Table 8 was tested by calculating the asymmetry of the peaks, A_S, according to Eq. (7) [31]. In Eq. (7) a_c and b_c are the distances between the elution volume of the peak maximum and the elution volume at 10% of the peak height after and before peak maximum, respectively.

Table 9
Effect of the resin matrix and eluent composition on the retention factor, k, the width of the peak base, w_b, the separation factor, α, and peak resolution, R_S, of rhamnose and xylose separation [29]

Resin	Ethanol in eluent (wt%)	D_{ax} (10^7 m^2/s)	k		w_b (cm^3)		α	R_S	Figure
			Rhamnose	Xylose	Rhamnose	Xylose			
SCE Na^+ ×8	0.0	0.36	0.34	0.44	10.1	9.4	1.28	0.19	5A
SCE Na^+ ×5.5	0.0	1.6	0.73	0.84	18.7	18.1	1.15	0.12	4A
SCE Na^+ ×5.5	9.6	1.6	0.78	0.97	22.5	22.2	1.24	0.16	4B
SCE Na^+ ×4	0.0	1.6	0.79	0.89	18.1	17.9	1.13	0.13	5B
SCE Ca^{2+} ×8	0.0	0.35	0.44	0.42	16.9	13.4	1.05	0.03	5D
SCE Ca^{2+} ×4	0.0	0.35	0.82	0.80	10.8	10.5	1.03	0.04	5E
WCE Na^+ ×6	0.0	1.6	0.50	0.82	15.9	19.4	1.65	0.38	5C
WCE Na^+ ×4	0.0	1.6	0.79	1.1	16.5	19.2	1.40	0.37	4C
WCE Na^+ ×4	9.5	1.5	0.94	1.4	17.8	22.1	1.52	0.44	4D

Parameters have been calculated from experimental data shown in Figs. 4 and 5.

$$A_S^2 = \left(\frac{a_c}{b_c}\right)^2 \quad (7)$$

4. Results and discussions

4.1. Sorption

The sorption of water–ethanol–sugar in the SCE and WCE resins is illustrated in Fig. 1. It is seen from Fig. 1 that sorption of water decreases with increasing ethanol concentration. At the same time ethanol sorption increases. According to Tiihonen et al. [7,13,14] the amount of water decreases in the SCE and WCE resins consistently, whereas the amount of ethanol goes through maximum or obtains a constant level. Furthermore, the resins are selective for water, the WCE resin being more selective than the SCE resin. A more detailed analysis about aqueous ethanol sorption in the SCE and WCE resins is given in Refs. [7,13].

Sugar sorption seems to decrease in Fig. 1, when alcohol is added to eluent. In fact, the case is opposite i.e. sugar sorption increases with the increasing ethanol concentration [14]. The decreasing trend in sugar sorption simply reflects the decreasing sugar concentration with the increasing ethanol content of the solvent. The effect of ethanol in sugar sorption is treated in detail in Refs. [5,6,14].

The critical part of the chromatographic column calculations is the proper description of the sorption equilibria of all components in a multicomponent mixture. In this paper, the NRF model was chosen because of its versatility as explained in the next section. Examples of the sorption are shown in Fig. 1. The data is plotted against the sugar-free solvent composition. In Fig. 1 the sugar concentration values vary between data points. Therefore, the calculated multicomponent sorption values cannot be represented as smooth lines, and they are given as open symbols instead. As seen in Fig. 1 and Table 5, multicomponent sorption can be successfully correlated by the present sorption equilibrium model. The calculated sorption data of all components in the SCE resin fit with good quality to the experimental data. In the WCE resin the calculated and experimental data, in general, coincide soundly, except for ethanol and rhamnose sorption. The stronger deviation of ethanol in the WCE resins is related to the difficulties encountered in accurately calculating the trend of ethanol sorption at higher ethanol concentrations in Ref. [7]. On the other hand, it should be noted that the sorbed amount of ethanol is significantly lower in the WCE resins than in the SCE resins causing scattering of the experimental sorption data in the WCE resin as mentioned in Ref. [7]. Overprediction of rhamnose is a result of fitting procedure needed to adequately predict both the isotherm and chromatographic data as explained earlier in this paper. However, it has been shown in Ref. [7] that the NRF model is applicable to different polymer systems such as strong and weak cation-exchangers.

In some cases the thermodynamic isotherm model applied in column calculation can reduce the experimental work needed for isotherm measurements. With the column calculation it is possible to test stationary phases which differ from each others only by one property, such as resins in the same ionic form but at different cross-link densities, without need to measure the entire isotherm. For example, sorption at given cross-link density of strong or weak cation-exchangers can be calculated, if experimental data and a valid thermodynamic model on one cross-link density are available [7,13,14].

4.2. Chromatography

Two approaches were utilized in studying chromatographic behavior of the model system. Firstly, the experimental data and the peaks fitted to the experimental data are presented. The effect of increased ethanol concentration in the eluent and the influence of the cation-exchanger type on chromatographic separation of rhamnose and xylose are shown in Figs. 3 and 4 and Table 9. The chromatograms of large pulses with high sugar concentrations are illustrated in Fig. 3 and those of small pulses with low sugar concentrations in Fig. 4. The effects of cross-link density and ionic form for experimental chromatographic data are shown in Fig. 5 and Table 9. In Figs. 3–5 both experimental chromatographic peaks and calculated peaks are illustrated.

Secondly, in addition to the fitting of the chromatographic peaks to the experimental data also independent simulations were carried out by using

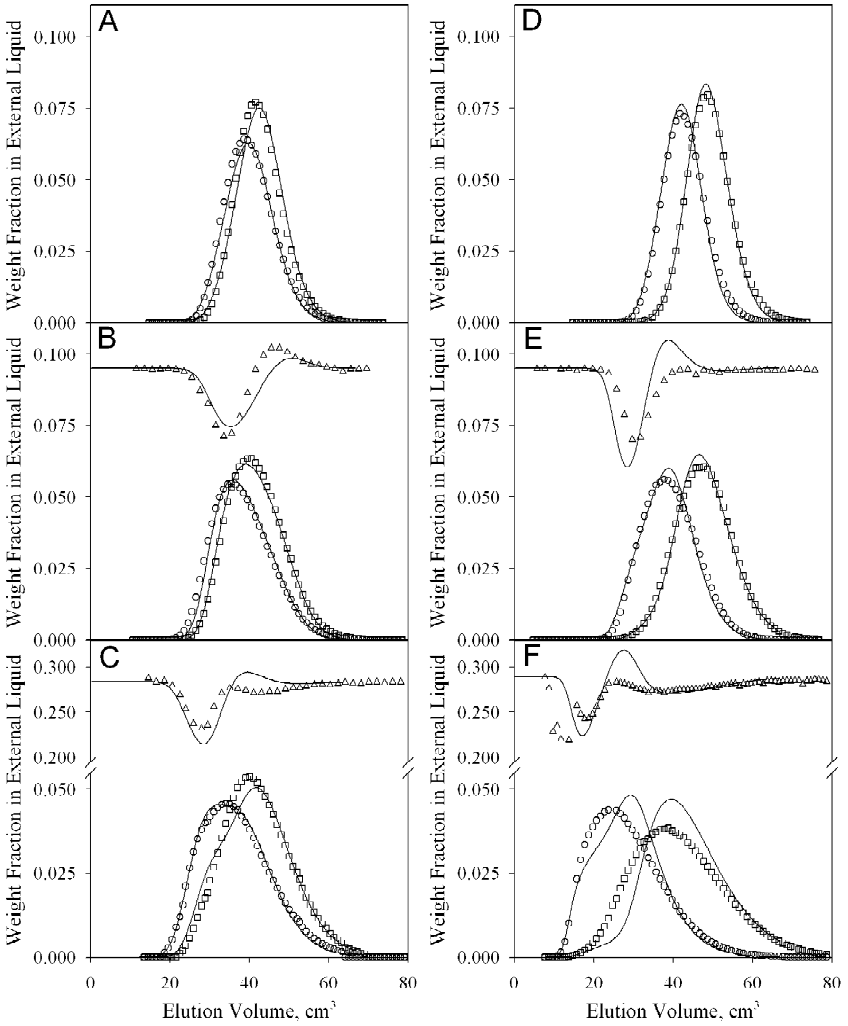

Fig. 3. Chromatograms of rhamnose and xylose at different eluent compositions. (A,B,C) SCE in Na^+ form, ×5.5; (D,E,F) WCE in Na^+ form, ×4. Eluent composition: (A,D) water; (B,E) about 10 wt% aqueous ethanol; (C,F) about 30 wt% aqueous ethanol. Bed volume in water was 60 cm^3. Flow-rate was 1 cm^3/min. Feed volume was 10–16% of the bed volume. Feed concentration of rhamnose and xylose was 16 and 18 wt%, respectively. Open symbols represent experimental data points and lines represent calculated results. Circles are for rhamnose, squares for xylose and triangles for ethanol.

constant column parameters. The column porosity, the bed size, the stationary phase bead diameter, the flow-rate as well as the sample concentrations and volume were all kept constant (Table 10). Dilute samples, small sample volumes and slow flow-rate were used to meet the requirements of the method of moments used in parameter estimation [30]. The constant column parameters enable a direct way to compare the separation efficiency between the SCE resins and the WCE resins (Fig. 6). Moreover, the dilute samples and small sample volumes enable to illustrate the effect of the resin deswelling on the mass transfer rate, i.e. on the solid-phase diffusion coefficients of the sugars. In these conditions the change of ϕ_p^S is negligible, and according to Eq. (6), D_i^S stays constant (Table 8). The B factor in Eq. (6) for independent simulation data has been estimated based on the values shown in Table 2.

According to the experimental and calculated results, the chromatographic separation of sugars is

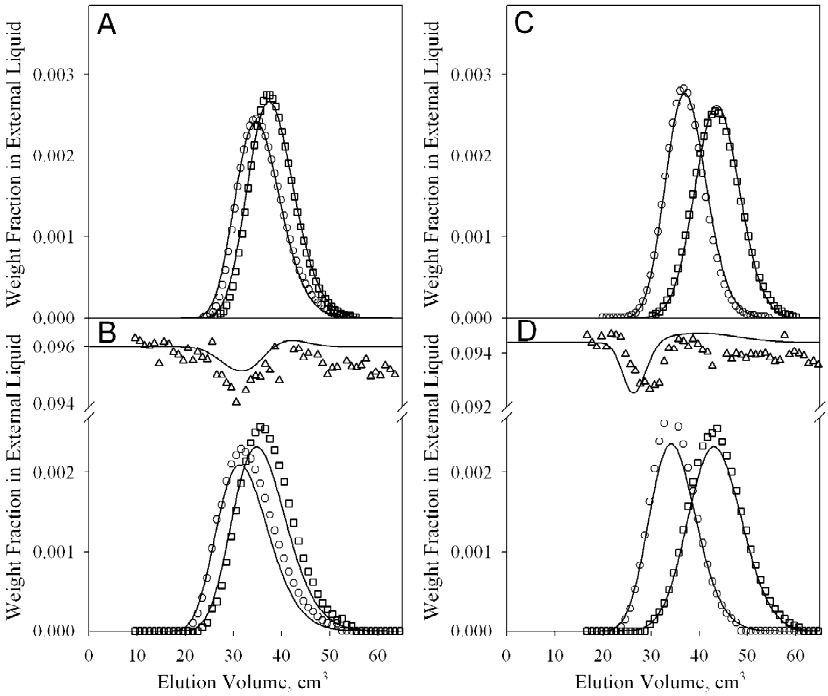

Fig. 4. Chromatograms of rhamnose and xylose at different eluent compositions. (A,B) SCE in Na^+ form, ×5.5; (C,D) WCE in Na^+ form, ×4. Eluent composition: (A,C) water; (B,D) about 10 wt% aqueous ethanol. Bed volume in water was 60 cm^3. Flow-rate was 1 cm^3/min. Feed volume was 0.8–1.0% of the bed volume. Feed concentration of rhamnose and xylose was 6.0 and 5.4 wt%, respectively. Open symbols represent experimental data points and lines represent calculated results. Circles are for rhamnose, squares for xylose and triangles for ethanol.

strongly affected by the eluent composition (Figs. 3, 4 and 6 and Tables 8 and 9) and the stationary phase properties (Figs. 3–6 and Tables 8 and 9). Increasing amount of ethanol in the eluent enhances the peak separation between the sugars studied. In fact, enhanced retention differences of carbohydrates in ion-exchange resins at aqueous alcohol eluents can be considered as a common knowledge [6]. In the case of rhamnose and xylose the enhanced separation at increased ethanol concentration can be related to the hydrophilicity difference between the sugars. Rhamnose solubility in water is only 39.8 wt% whereas the solubility of xylose is 55.1 wt% at 298 K [8,20]. Thus, less hydrophilic rhamnose has weaker affinity than xylose towards the hydrophilic stationary phases. The difference in the distribution of the two sugars increases further in the presence of the ethanol co-eluent, because rhamnose interacts more strongly with ethanol as shown by the less positive interaction energy values in Table 4. Therefore, ethanol increases the rhamnose activity in the mobile phase less than that of xylose and enhances the sorption difference between the two sugars. The increased sorption difference in ethanol solutions can be seen from the chromatographic parameters in Table 9 and Fig. 6. The increased separation factor, which is equal to the increased distribution constant ratio, indicates larger sorption difference of sugars in aqueous ethanol [29].

The hydrophilicity can be the decisive factor in non-specific partition chromatography but the situation changes when also other interactions are introduced. This is seen in Fig. 5D, E where rhamnose–xylose separation with the SCE Ca^{2+} resins are tested. Both sugars have the same elution volume. The reduced separation efficiency may stem from the complex forming ability of the divalent counter-ion. Usually rhamnose and xylose are not considered as complex forming sugars [32], but even a slightly stronger complexing ability in favor of rhamnose can

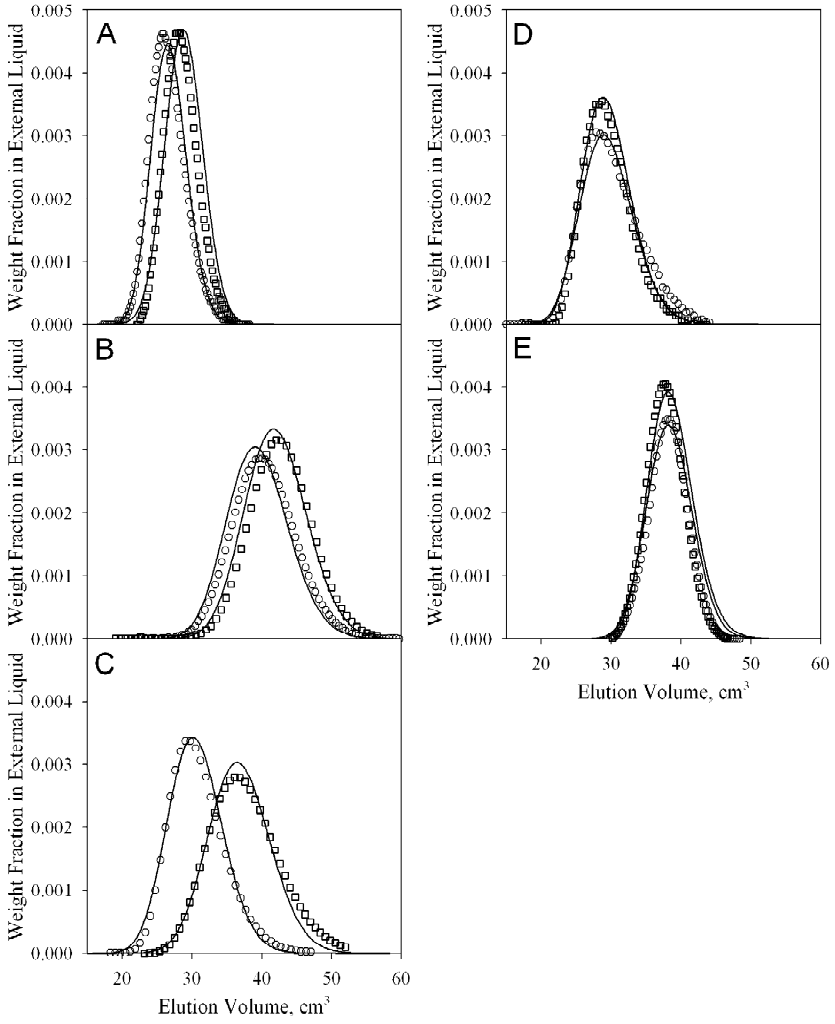

Fig. 5. Chromatograms of rhamnose and xylose in water at different ionic forms and cross-link densities. (A,B) SCE in Na^+ form; (C) WCE in Na^+ form; (D,E) SCE in Ca^{2+} form. Cross-link density: (A,D) ×8; (C) ×6; (B,E) ×4. Bed volume in water was from 52 to 60 cm^3. Flow-rate was 0.25 cm^3/min (A,D,E) or 1 cm^3/min (B,C). Feed volume was 0.8–1.0% of the bed volume. Feed concentration of rhamnose and xylose was 6.0 and 5.4 wt%, respectively. Open symbols represent experimental data points and lines represent calculated results. Circles are for rhamnose and squares for xylose.

increase the rhamnose retention and make the separation inefficient.

It can be readily seen from Table 9 and Figs. 3 and 4 that the separation of rhamnose from xylose is significantly better in the WCE than in the SCE. The WCE has stronger affinity toward water than the SCE [7] and the sorption difference of rhamnose and xylose in the WCE compared to the SCE is further increased due to the hydrophilicity difference between sugars as explained earlier in this paper. Moreover, the WCE resin is more water selective than the SCE resin [7]. The stronger water selectivity improves the separation of different hydrophilicity sugars more in the WCE resin than in the SCE at the equal eluent composition when moving from water to aqueous ethanol solutions. The more effective separation is even more evident from the simulation results in Fig. 6 and Table 8. The separation factor and resolution of the WCE in water and in 10 wt% ethanol are similar or higher than those of SCE in

Table 10
Conditions in the simulated chromatographic runs presented in Table 8 and Fig. 6

Bed height (cm)	Column diameter (cm)	Bead diameter (mm)	Porosity
30	1.6	0.1	0.40

Sample concentration (wt%)		Sample volume (cm^3)	Flow-rate (cm^3/min)
Rhamnose	Xylose		
6.0	6.0	0.5	0.25

40 wt% ethanol at the equal cross-link densities (Fig. 6). Moreover, it can be seen from Table 8 that the elution volumes (see retention factors, *k*) in the WCE are smaller and peaks are narrower below 10 wt% ethanol than those of the SCE above 30 wt% ethanol. The WCE shrinks considerably more than the SCE in ethanol containing eluents (Table 2 and Ref. [7]). Thus, the ethanol concentration should be kept even lower, when the WCE resins are used.

The simulated data of Fig. 6, where linear conditions and slow flow-rate are applied, imply that the increased cross-link density enhances separation. The increased capacity of the high cross-linked resins due to the lower solvent contents may explain the observed enhancement. A small improvement in separation (resolution) have been achieved with the highest cross-linkage WCE ×6 in 0–10 wt% ethanol and SCE ×8 in 10–30 wt% ethanol when only cross-link densities have been compared. Up to a system specific cross-linkage level this is valid also for non-linear conditions met with concentrated sample solutions, with larger sample volumes, and with higher flow-rates. Above that level, mass transfer kinetics become slow causing peak tailing, which starts to disturb separation [1,10]. An example of the cross-link density effect on the peak shape is seen in Fig. 5. The sugar peak tailing in the 8 wt% DVB resin (Fig. 5D) is more pronounced compared to the peak shape in the 4 wt% DVB resin (Fig. 5E). The exchangers having lower cross-link densities have more open structure and they swell more than the higher cross-linkage exchangers. This can be utilized by using the lower cross-link density exchangers at more concentrated ethanol solutions. On the other hand, it should be noted that at certain ethanol concentration the resin swelling becomes independent of cross-link density [7,13]. However, the effect of slowing diffusivity is seen from Table 8. Moreover, the effect of the strong deswelling of the WCE is evident at 20 wt% ethanol eluent, where the lower cross-linkage resin ×4 has overcome ×6 in resolution (Fig. 6A).

A specific feature of separation in eluent mixtures are the system peaks that arise from the local concentration changes of the eluent components due to the sample components [10]. In the present case, the system peaks are observed from the change of the ethanol concentration due to rhamnose and xylose in Figs. 3B, C, E, F and 4B, D. The number of system peaks equals the number of sample components plus one in the case of a binary solvent eluent. One of the system peaks arises from the

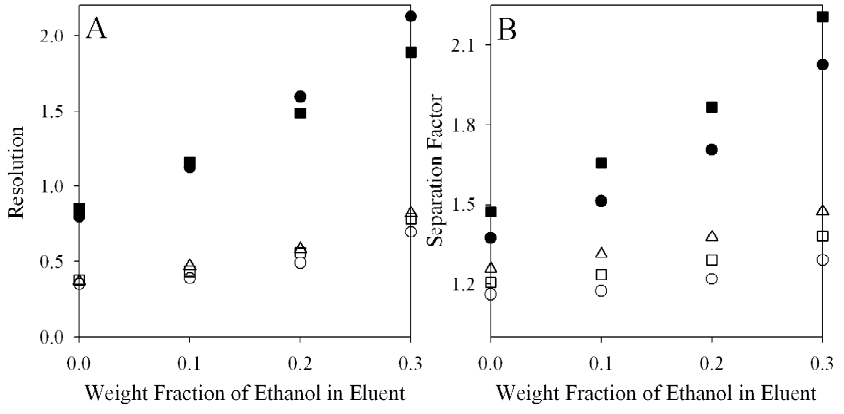

Fig. 6. Separation parameters of rhamnose–xylose separation from simulated data when small pulses and slow flow-rate was applied. △, SCE ×8; □, SCE ×5.5; ○, SCE ×4; ■, WCE ×6; ●, WCE ×4. All resins were in the Na^+ form. Bed volume was 60 cm^3. Flow-rate was 0.25 cm^3/min. Feed volume was 0.8% of the bed volume. Feed concentration of rhamnose and xylose was 6.0 wt%.

retention of the ethanol co-eluent. The other peaks elute with each sample component [10]. The experimental data and the simulated chromatograms indicate that the marked decrease of ethanol concentration before and during the elution of rhamnose is due to the sorption properties of ethanol. The system peaks eluting with the sample components seem to be much smaller and are partly covered by the above mentioned ethanol sorption peak. Thus, the maximum in the ethanol concentration, observed in some cases in Fig. 3, can result from the overlapping of the system peaks. Generally, the column model predicts correctly the location of the ethanol peak minimum and also gives reasonable estimates for the ethanol concentration, although the magnitude of the ethanol concentration changes is in some cases overpredicted.

Thus, the distortion of the simulated sugar peaks at high concentrations with large sample size (Fig. 3C, F) can be attributed to the discrepancies between the measured and calculated ethanol peaks. In Fig. 3F, for example, the ethanol weight fraction passes through a minimum at elution volume of 17 cm^3, and increases rapidly from 23 to 32 wt% (system peak due to the sorption properties of ethanol). As a consequence, the sum of the weight fractions of the sugars and water (not shown) must decrease, which is observed as distorted sugar peaks. It is possible that the real volume change of the resin and the predicted volume change deviate and this deviation causes the difference between measured and calculated peaks. On the other hand, the mixing of liquid components can be stronger than expected by the model, leading to smaller concentration gradients between liquid and solid-phase.

5. Conclusions

The chromatographic separation of rhamnose and xylose in water and in aqueous ethanol eluents with strong and weak cation-exchangers are reported. The weak cation-exchanger showed significant improvement in separation efficiency over the strong cation-exchanger between sugars having different hydrophilicities. Furthermore, the moderate addition of ethanol on eluent increased the retention differences between the sugars studied.

The thermodynamic sorption model was successfully implemented in column calculation. The rate-based column simulation model, which accounts for the volume changes of the stationary phase and the concentration dependence of the mass transfer coefficient, was able to quantitatively describe the chromatographic performance at the relatively wide sugar concentration range.

6. Nomenclature

a	particle area to volume ratio, 1/m
AAD	absolute average deviation
a_c	distance from peak maximum to 10% of the peak maximum, m^3
A_S	asymmetry factor
a_i(l)	liquid phase activity
a_i(s)	resin phase activity
d_{av}	average bed diameter in sodium form, m
b_c	distance from 10% of the peak maximum to peak maximum, m^3
B	coefficient in Eq. (6)
D_{ax}	axial dispersion coefficient, m^2/s
D_i^{aq}	diffusion coefficient in water, m^2/s
D_i^S	solid-phase diffusion coefficient, m^2/s
d_p	particle diameter, m
d_p^0	particle diameter at the initial degree of swelling, m
G	shear modulus, Pa
k	retention factor
K_{el}	elastic parameter, Pa
k_i^{eff}	effective mass transfer coefficient, m/s
N	number of data points
n	number of solvent and solute components
q	polymer swelling ratio
q_i	surface parameter
R	gas constant, J/(mol K)
R^2	coefficient of determination
R_S	peak resolution
r_i	size parameter
T	temperature, K
t	time variable, s
t_0	injection time, s
u	superficial velocity, m/s
V_M	retention volume of non-adsorbing component, m^3

$V_{m,i}$	partial molar volume, m^3/mol
$V_{equiv,i}$	equivalent volume of the polymer, m^3/equiv
$V_{R,i}$	retention volume, m^3
w_b	peak width, m^3
x_i	mole fraction
z	axial coordinate, m
z_i	coordination number

Greek letters

α	separation factor
γ_i	symmetric activity coefficient
ΔE_{ij}	interaction energy parameter, J/mol
ϵ	bed porosity
ϵ^0	bed porosity at the initial degree of swelling
π_{el}	elastic pressure, Pa
ϕ_i^L	volume fraction in liquid phase
ϕ_i^S	volume fraction in resin phase
ϕ_p^S	volume fraction of resin matrix
$\hat{\phi}_i^S$	volume fraction in resin at sorption equilibrium

Acknowledgements

The experimental work of laboratory technician Anne Hyrkkänen is gratefully acknowledged. The financial support from the National Technology Agency (TEKES, Finland) and Danisco A/S (Finland) is gratefully acknowledged. The Finex resins were kindly donated by Finex Oy (Finland). J. Tiihonen and T. Sainio acknowledge personal grant from the Finnish Cultural Foundation, South-Carelian Province Foundation. Furthermore, J. Tiihonen acknowledges personal grants from Emil Aaltosen Säätiö (foundation, Finland) and Tekniikan edistämissäätiö (foundation, Finland).

References

[1] H. Welstein, C. Sauer, in: D. Naden, M. Streat (Eds.), Ion Exchange Technology, Horwood, Chichester, UK, 1984, p. 463.
[2] R. Kunin, Amber-Hi-Lites 174 (1984) 485.
[3] X. Lancrenon, D. Herve, Sugar Technol. Rev. 14 (1988) 207.
[4] A. Kärki, H. Heikkilä, J. Jumppanen, J. Tiihonen, T. Tervala, N. Mäyrä, V. Ravanko, H. Paananen, E. Paatero, PCT Int. Appl. WO 0227038 (2002).
[5] O. Samuelson, Ion Exchange Separation in Analytical Chemistry, in: Wiley, New York, 1963, p. 138.
[6] O. Samuelson, in: J.A. Marinsky (Ed.), Ion Exchange: A Series of Advances, Vol. 2, Marcel Dekker, New York, 1969, p. 167.
[7] J. Tiihonen, I. Markkanen, A. Kärki, P. Äänismaa, M. Laatikainen, E. Paatero, Chem. Eng. Sci. 57 (2002) 1885.
[8] N. Gabas, T. Carillon, N. Hiquily, J. Chem. Eng. Data 33 (1988) 128.
[9] C.J. Moye, in: R.S. Tipson, D. Horton (Eds.), Advances in Carbohydrate Chemistry and Biochemistry, Vol. 27, Academic Press, New York, 1972, p. 85.
[10] G. Guichon, S.G. Shirazi, A.M. Katti, Fundamentals of Preparative and Nonlinear Chromatography, Academic Press, Boston, MA, 1994, pp. 99, 207–213.
[11] O. Lisec, P. Hugo, A. Seidel-Morgenstern, J. Chromatogr. A 908 (2001) 19.
[12] M. Mazzotti, B. Neri, D. Gelosa, M. Morbidelli, Ind. Eng. Chem. Res. 36 (1997) 3163.
[13] J. Tiihonen, M. Laatikainen, I. Markkanen, E. Paatero, Ind. Eng. Chem. Res. 38 (1999) 4832.
[14] J. Tiihonen, M. Laatikainen, I. Markkanen, E. Paatero, J. Jumppanen, Ind. Eng. Chem. Res. 38 (1999) 4843.
[15] C. Panayiotou, J.H. Vera, Fluid Phase Equilib. 5 (1980) 55.
[16] D.S. Abrams, J.M. Prausnitz, AIChE J. 21 (1975) 116.
[17] G.M. Gusler, Y. Cohen, Ind. Eng. Chem. Res. 33 (1994) 2345.
[18] J. Tiihonen, I. Markkanen, M. Laatikainen, E. Paatero, J. Appl. Polym. Sci. 82 (2001) 1256.
[19] Z. Li, R.T. Yang, AIChE J. 45 (1999) 196.
[20] Beilstein's Handbuch, 4. Aufl. I. 865.
[21] H. Uedaira, H. Uedaira, Bull. Chem. Soc. Jpn. 42 (1969) 2137.
[22] A.M. Peres, E.A. Macedo, Entropie 71 (1997) 202.
[23] R.C. Reid, J.M. Prausnitz, B.E. Poling, The Properties of Gases and Liquids, in: 4th ed., McGraw-Hill, New York, 1987, p. 317.
[24] A.C. Hindmarsh, in: R.S. Stepleman (Ed.), Odepack, a Systematized Collection of ODE Solvers, Scientific Computing, North-Holland Publishing, Amsterdam, 1983.
[25] W.E. Schiesser, The Numerical Method of Lines: Integration of Partial Differential Equations, Academic Press, San Diego, 1991.
[26] S.F. Chung, C.Y. Wen, AIChE J. 14 (1968) 857.
[27] P. Meares, in: J. Crank, G.S. Park (Eds.), Diffusion in Polymers, Academic Press, London, 1968, p. 404.
[28] M. Goto, S. Goto, Sep. Sci. Technol. 22 (1987) 1503.
[29] L.S. Ettre, Pure Appl. Chem. 65 (1993) 819.
[30] D.M. Ruthven, Principles of Adsorption and Adsorption Processes, in: John Wiley & Sons, New York, 1984, p. 240.
[31] E.L. Johnson, R. Stevenson, Basic Liquid Chromatography, in: Varian Associates Inc, California, 1978, p. 48.
[32] J. Tiihonen, I. Markkanen, E. Paatero, Chem. Eng. Comm. 189 (2002) 995.